# Nonlinear backstepping and model predictive control for gridconnected permanent magnet synchronous generator wind turbines

# Adil El Kassoumi<sup>1</sup>, Mohamed Lamhamdi<sup>1</sup>, Ahmed Mouhsen<sup>2</sup>, Mohammed Fdaili<sup>3</sup>, Imad Aboudrar<sup>4</sup>, Azeddine Mouhsen<sup>1</sup>

<sup>1</sup>Department of Radiation-Matter and Instrumentation, Faculty of Sciences and Technology Settat, Hassan First University, Settat, Morocco

<sup>2</sup>Department of Engineering, Industrial Management and Innovation, Faculty of Sciences and Technology Settat, Hassan First University, Settat, Morocco

<sup>3</sup>Research Center in Sciences and Technologies of Engineering and Health, National Higher School of Arts and Crafts Mohammed V University, Rabat, Morocco

<sup>4</sup>Engineering and Sustainable Development Research Team, EST of Dakhla Ibn Zohr University, Agadir, Morocco

# **Article Info**

# Article history:

Received Aug 31, 2024 Revised Aug 11, 2025 Accepted Sep 15, 2025

# Keywords:

Backstepping control
Direct-drive permanent magnet
synchronous generator
Finite control set model
predictive control
Nonlinear backstepping
Wind turbine

#### **ABSTRACT**

This research investigates and compares two nonlinear current-control strategies, backstepping control (BSC) and finite control set model predictive control (FCS-MPC) for machine-side and grid-side converters in grid-connected direct-drive permanent magnet synchronous generator (DD-PMSG) wind turbines. Addressing the control challenges in wind energy systems with varying speeds, the study aims to determine which strategy offers superior performance under identical operating conditions. The nonlinear BSC regulates stator and grid currents using Lyapunov-based techniques, while FCS-MPC leverages model predictions to select optimal switching states based on a cost function. A comprehensive simulation using MATLAB/Simulink is conducted, analyzing each controller's transient behavior, steady-state response, torque ripple, and power quality total harmonic distortion (THD). Results show that FCS-MPC achieves faster convergence, lower overshoot, and superior power quality compared to BSC, though it requires higher computational resources. Statistical validation supports the robustness of FCS-MPC under parameter uncertainties. This work contributes a structured comparison of advanced nonlinear strategies for PMSG-based wind turbines and provides a foundation for future implementations in real-time embedded control systems. Future directions include experimental validation and hybrid model predictive controllerartificial intelligence (MPC-AI) control frameworks.

This is an open access article under the <u>CC BY-SA</u> license.



5091

# Corresponding Author:

Adil El Kassoumi

Department of Radiation-Matter and Instrumentation, Faculty of Sciences and Technology Settat, Hassan First University

BP 577, Settat, Morocco

Email: a.elkassoumi@uhp.ac.ma

# 1. INTRODUCTION

In recent years, the imperative transition towards sustainable energy practices has fueled integrating renewable energy sources into electrical systems, marking a paradigm shift in the global energy landscape. Among these sources, wind energy stands out as a prominent contributor, harnessing the power of the wind to generate electricity cleanly and efficiently [1]. This paper delves into the domain of wind energy

Journal homepage: http://ijece.iaescore.com

conversion, focusing on grid-connected direct-drive permanent magnet synchronous generator (DD-PMSG) as a key solution in this transformative era. However, the grid-integration of renewable power sources poses significant challenges, including dynamic stability, parameter variation, and grid synchronization requirements, which demand sophisticated control strategies.

Morocco, like many nations, has embraced the potential of wind energy to diversify its energy mix and reduce dependence on conventional fossil fuels [2]. Data recently collected by the Ministry for the Transition to Energy and Sustainable Development, the nation's wind power capacity has increased at an astounding rate. The REmap report published in November 2023 states that Morocco's total installed wind capacity stood at 2.16 GW with an ambitious objective to reach 5.8 GW by 2030 [3]. This significant contribution, which currently represents approximately 18% of the country's total electricity generation capacity, underscores Morocco's commitment to achieving its renewable energy targets and aligns with its plans to further expand its wind power capabilities [4].

Ensuring optimal performance and stability of such generators requires sophisticated control strategies for both the machine-side converter (MSC) and the grid-side converter (GSC). This research focuses on advancing the understanding of current control techniques in the context of DD-PMSG systems, employing filed and voltage-oriented controls [5]. The academic literature reveals a progressive evolution in control techniques for permanent magnet synchronous generator (PMSG) systems. Early studies predominantly focused on vector control methods, including field-oriented control (FOC) and direct torque control (DTC). These approaches provided foundational insights into controlling torque and flux effectively, which are critical for the efficient operation of PMSGs. For example, FOC and DTC established control mechanisms that improved the accuracy and efficiency of PMSG systems, though they encountered challenges such as torque ripples and variable switching frequencies [6]. With the growing integration of PMSGs into grid-connected renewable energy sources, research priorities shifted toward grid synchronization and power quality enhancement. This transition emphasized the role of reactive power control in maintaining grid stability and mitigating disturbances. Proportional-integral (PI) controllers have been widely adopted due to their simplicity and steady-state performance; however, their limitations under dynamic conditions and parameter variations are well-documented [7], [8].

Advanced control methodologies, like sliding mode control (SMC) and backstepping control, have been investigated to overcome the constraints of traditional controllers. SMC is recognized for its robustness against system uncertainties and external disturbances but suffers from chattering effects, potentially impacting generator stability [7]–[12]. Backstepping control, while offering stability guarantees, becomes computationally complex as system orders increase. Similarly, artificial intelligence (AI) based methods such as fuzzy logic and neural networks have been employed to create adaptive control laws, but their reliance on extensive training data and computational resources makes them less suited for real-time control applications [13].

AI-driven control methodologies, including fuzzy logic systems and neural networks (NN), and deep reinforcement learning (DRL) are gaining increasing attention in wind turbine control due to their adaptability and data-driven nature. These methods can learn complex nonlinear relationships, adapt to changing conditions, and enhance control robustness. While they offer promising alternatives to conventional optimization-based techniques like particle swarm optimization (PSO) and genetic algorithm (GA) [14], which often suffer from local optima and high computational costs, AI methods also present challenges related to training data requirements, real-time deployment, and hardware compatibility [15]. To provide a clearer overview of control strategies, Table 1 presents a comparative analysis based on key criteria such as accuracy, robustness, computational demand, and real-time feasibility. This comparison highlights the trade-offs between traditional, optimization-based, and intelligent control methods.

Despite advancements in control strategies for grid-connected PMSG wind turbines, challenges remain with classical PI controllers, and advanced methods like backstepping and model predictive control (MPC) face limitations. While backstepping control offers robustness for nonlinear systems, its computational complexity can hinder implementation in higher-order systems. On the other hand, MPC provides strong performance in handling multi-variable constraints but struggles with its reliance on accurate models and high computational demands, limiting real-time applicability. These gaps underscore the need for a detailed comparison of Backstepping and MPC strategies, focusing on their trade-offs in robustness, computational efficiency, and adaptability for dynamic grid-connected PMSG systems. This research aims to address these gaps through a comparative analysis of both control methods.

This research paper is methodically structured to provide a thorough examination of current control strategies in DD-PMSGs. Section 1 the introduction, underscores the critical need for precise current control in DD-PMSGs, critiques the limitations of conventional and advanced control methods, while also outlining the research objectives and contributions. In section 2 the paper delineates the architecture of the wind turbine system (WTS), including key components and their interactions. This section provides a detailed

mathematical model of the DD-PMSG, encompassing stator voltage and current equations, and extends to modeling the GSC-connected grid. Section 3, where it introduces and analyzes the concept, the design methodology, the system stability, and performance characteristics of the proposed nonlinear Backstepping controller. The paper then progresses to section 4, which explicates the principles of MPC, the implementation and the design processes of finite control set model predictive control (FCS-MPC). Besides its computational complexity and performance efficacy. This is followed by section 5 describes the simulation setup and presents results for various system conditions, facilitating a comparative performance analysis of the two control strategies. The paper ends with a conclusion, where it synthesizes the key findings, emphasizes the contributions of the research, discusses the potential real-world applications of the proposed control strategies, and proposes future research directions for the advancement of PMSG control techniques.

TD 11 1	~	. 11 0	. 1	
Table I	Comparative	table of	control	ctratemiec
Table 1.	Comparative	table of	COHUOI	suawgics

Control techniques	Accuracy	Robustness	Computational complexity	Real-time feasibility	Adaptability to parameter changes
PI controller	Moderate	Low to moderate	Low	Excellent	Low
Backstepping control (BSC)	High	High	Moderate	Good	Moderate
SMC	Very high	Very high	Moderate to high	Moderate	High
FCS-MPC	Very high	High	High	Requires	High
				optimization	
AI-based control	Potentially very high	High (if trained well)	Very high	Depends on	Very high
(e.g., Fuzzy/NN)				hardware	

#### 2. DD-PMSG WIND TURBINE SYSTEM MODELING

Figure 1 illustrates the design of the proposed WTS. It typically encompasses three primary components: the wind turbine, a DD-PMSG, and a power electronic interface for grid connection, which in this case includes a back-to-back converter system (BBCS). This BBCS is essentially composed of two parts: a rectifier (MSC) and an inverter (GSC), connected by a DC link. In order for the DD-PMSG's variable-frequency output to be properly turned into the fixed-frequency energy needed for grid compatibility, this setup is very important. The machine-side converter is responsible for transforming the alternating current (AC) power produced by the PMSG into direct current (DC) power. Subsequently, the grid-side converter takes this DC power and inverts it back into AC power, matching the grid frequency. This process is crucial for the regulation of both active and reactive power and for ensuring synchronization with the grid, thus facilitating a stable and efficient integration of wind energy into the electrical grid system [16].

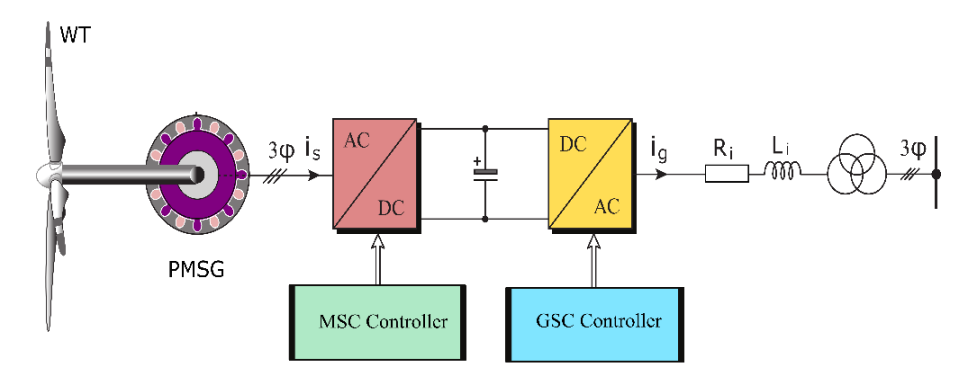


Figure 1. The suggested WTS's architecture

# 2.1. Wind turbine model

The mechanical power extracted by a wind turbine from the wind can be represented using (1) [17]:

$$P_{mec} = \frac{1}{2} \rho A V^3 C_p(\lambda, \beta) \tag{1}$$

Air density is denoted by  $\rho$ , A represents the turbine rotor's swept area  $A = \pi R^2$ , V signifies wind speed,  $C_n(\lambda, \beta)$  indicates the power coefficient,  $\beta$  refers to the blade pitch angle, and  $\lambda$  denotes the tip-speed ratio.

The power coefficient  $C_p(\lambda, \beta)$  is a crucial factor in this equation, representing the efficiency of the wind turbine in converting wind energy into mechanical energy [18]. That is conditional on the tip-speed-ratio  $\lambda$ , which is defined as:

$$\lambda = \frac{\Omega R}{V} \tag{2}$$

$$C_p(\lambda, \beta) = \frac{1}{2} \left( \frac{116}{\lambda_i} - 0.4\beta - 5 \right) e^{\frac{-21}{\lambda_i}} + 0.0068\lambda$$
 (3)

with: 
$$\frac{1}{\lambda_i} = \frac{1}{\lambda + 0.08\beta} - \frac{0.035}{1 + \beta^3}$$

 $\Omega$  represents the rotor's angular velocity, while *R* is its radius.

#### 2.2. DD-PMSG model

In order to transform wind turbine mechanical energy into electrical energy, the DD-PMSG model is required. This model includes key electromagnetic equations and dynamics of the generator. The stator voltage equations in the d-q frame are [19]:

$$v_{ds} = R_s i_{ds} + \frac{d\psi_{ds}}{dt} - \omega_s \psi_{qs} \tag{4}$$

$$v_{qs} = R_s i_{qs} + \frac{d\psi_{qs}}{dt} - \omega_s \psi_{ds} \tag{5}$$

where the d-axis and q-axis parts of stator voltage are called  $v_{ds}$  and  $v_{qs}$ , respectively. The d-axis and q-axis parts of the stator current are called  $i_{ds}$  and  $i_{qs}$ . The d-axis and q-axis parts of stator flux linkage are called  $\psi_{ds}$  and  $\psi_{qs}$ , respectively. The stator resistance is denoted by  $R_s$ . The stator's electrical angular velocity is denoted by  $\omega_s$ .

The following are the flux linkage equations:

$$\psi_{ds} = L_d i_{ds} + \psi_f \tag{6}$$

$$\psi_{qs} = L_q i_{qs} \tag{7}$$

where  $L_d$  and  $L_q$  are the inductances of the stator's d-axis and q-axis. The permanent magnet flux linkage is denoted by  $\psi_f$ .

We can figure out the stator current behavior from these models. By switching the voltage equations around and adding the flux coupling equations instead, we get:

$$\frac{di_{ds}}{dt} = \frac{1}{L_d} \left( v_{ds} - R_s i_{ds} + \omega_s L_{qs} i_{qs} \right) - \frac{\psi_f}{L_d} \omega_s \tag{8}$$

$$\frac{di_{qs}}{dt} = \frac{1}{L_a} \left( v_{qs} - R_s i_{qs} + \omega_s L_{ds} i_{ds} \right) \tag{9}$$

A crucial element of energy conversion, the electromagnetic torque can be calculated as:

$$T_{em} = \frac{2}{2} P(\psi_{ds} i_{qs} - \psi_{qs} i_{ds}) \tag{10}$$

The dynamic behavior of the generator is explained by (11):

$$J_{gen} \frac{d\Omega}{dt} = T_{mech} - T_{em} - B_{gen} \Omega \tag{11}$$

The electromagnetic torque is indicated by  $T_{em}$ , and P stands for the generator's number of pole pairs, the generator's moment of inertia is denoted by  $J_{gen}$ , The damping coefficient, which represents mechanical losses, is represented by  $B_{gen}$ , whereas the turbine torque is represented by  $T_{mech}$ .

### 2.3. DC link modeling

The rectifier and the inverter are connected by the DC link. The DC link voltage is given by [20]:

$$V_{dc} = \frac{1}{C_{dc}} \int (i_{rd} - i_{id})dt \tag{12}$$

The DC link's capacitance is represented by  $C_{dc}$ . The rectifier current is  $i_{rd}$ . The inverter current on the d-axis is denoted by  $i_{id}$ .

## 2.4. Grid-side converter (inverter) model

The inverter converts DC power back to AC for grid interconnection via RL filter. The grid voltage equations in the dq frame are [21]:

$$v_{dg} = v_{id} - R_i i_{dg} - L_i \frac{di_{dg}}{dt} + L_i \omega_g i_{qg}$$

$$v_{dg} = v_{iq} - R_i i_{qg} - L_i \frac{di_{qg}}{dt} - L_i \omega_g i_{dg}$$
(13)

$$v_{dg} = v_{iq} - R_i i_{qg} - L_i \frac{di_{qg}}{dt} - L_i \omega_g i_{dg}$$

$$\tag{14}$$

Here, the d-axis and q-axis components of the inverter voltage are denoted by  $v_{id}$  and  $v_{iq}$ , respectively, the d-axis and q-axis components of the inverter current are denoted by the  $i_{dg}$  and  $i_{qg}$ ,  $R_i$  and  $L_i$  are the resistance and inductance of the filter, and  $\omega_a$  is the electrical angular velocity of the grid.

# NONLINEAR BACKSTEPPING CONTROL OF THE DD-PMSG WIND TURBINE

Controlling the MSC and the GSC is a very important part of making sure that a wind energy conversion system (WECS) system works well and efficiently. For the MSC, its key function is to maximize wind energy capture. This is achieved by implementing maximum power point tracking (MPPT) based on the generator's speed, alongside managing torque or power control. Conversely, the GSC is responsible for a range of critical functions: it regulates the voltage of the DC bus, manages the grid's reactive power, ensures grid synchronization, and maintains operation during grid faults (fault ride-through (FRT)) [22]. A typical control scheme using a nonlinear backstepping strategy is given in Figure 2.

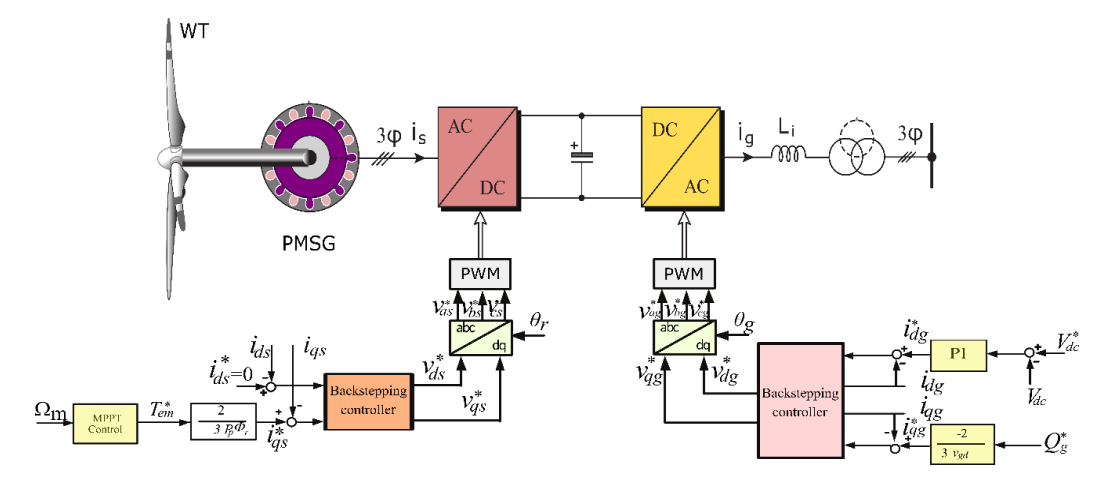


Figure 2. Nonlinear backstepping control for MSC and GSC

# 3.1. MSC control by nonlinear backstepping based on optimal torque control MPPT

The objective of the MSC is to control the PMSG to extract maximum power from the wind. This is achieved by adjusting the torque of the generator. Optimal torque control (OTC) is implemented for MPPT. The optimal torque reference  $(T_{opt})$  is derived based on the wind speed and the characteristics of the wind turbine.

Based on the connection between wind speed V and the tip speed ratio  $\lambda$ , and by substituting  $\lambda$  with its optimal value  $\lambda^{opt}$  and equating the power coefficient  $C_p$  to its maximum value  $C_p^{max}$  [23], we derive (15):

$$K^{opt} = \frac{1}{2} \rho \pi R^5 \frac{c_p^{max}}{\lambda^{opt^3}} \tag{15}$$

Thus, the reference for electromagnetic torque, denoted as  $T_{em}^{ref}$ , is formulated in the following manner:

$$T_{em}^{\ \ ref} = K^{opt} \Omega^2 \tag{16}$$

The reference currents are defined as:

$$\begin{cases} i_{ds}^* = 0 \\ i_{qs}^* = \frac{2}{3} \frac{1}{p_n \psi_r} T_{em}^* \end{cases}$$
 (17)

# 3.2. MSC control using nonlinear backstepping approach

From Figure 2, it can be seen that the stator currents can be controlled by  $v_{ds}$  and  $v_{qs}$ , hence the stator currents errors are expressed as [24]:

$$\begin{cases} \xi_d = i_{ds}^* - i_{ds} \\ \xi_g = i_{gs}^* - i_{gs} \end{cases}$$
 (18)

where  $i_{ds}^*$  and  $i_{qs}^*$  are the current component references. Based on (17) and (18), we can write:

$$\begin{cases}
\frac{d\xi_d}{dt} = -\frac{1}{L_d} \left( v_{ds} - R_s i_{ds} + \omega_r L_q i_{qs} \right) \\
\frac{d\xi_q}{dt} = i_{qs}^* - \frac{1}{L_q} \left( v_{qs} - R_s i_{qs} - \omega_r L_d i_{ds} - \omega_r \psi_r \right)
\end{cases}$$
(19)

The Lyapunov function is chosen as given in:

$$\begin{cases} W_{\alpha} = \frac{1}{2} \left( \xi_d^2 + \xi_q^2 \right) > 0 \\ \frac{dW_{\alpha}}{dt} = \xi_d \frac{d\xi_d}{dt} + \xi_q \frac{d\xi_q}{dt} \end{cases}$$
 (20)

Furthermore, coefficients  $Y_d$  and  $Y_q$  must be positive to ensure the system stability [25].

$$\frac{dW_{\alpha}}{dt} = -Y_d \xi_d^2 - Y_q \xi_q^2 < 0 \tag{21}$$

The stator currents tracking errors are achieved if only the following d/q voltage references are chosen:

$$\begin{cases} v_{ds}^* = L_d Y_d \xi_d + R_s i_{ds} - \omega_r L_q i_{qs} \\ v_{qs}^* = L_q Y_q \xi_q + R_s i_{qs} + \omega_r L_d i_{ds} + \omega_r \psi_r + L_q \frac{d i_{qs}^*}{dt} \end{cases}$$
(22)

# 3.3. GSC control using nonlinear backstepping approach

The errors in the direct and quadrature grid currents can be described using the following formulas [26]:

$$\begin{cases}
\Gamma_d = i_{dg}^* - i_{dg} \\
\Gamma_q = i_{qg}^* - i_{qg}
\end{cases}$$
(23)

using (13) and (14), we obtain:

$$\begin{cases}
\frac{d\Gamma_{d}}{dt} = \frac{di_{dg}^{*}}{dt} - \frac{1}{L_{i}} \left( v_{id} - v_{g} - R_{i}i_{dg} + L_{i}\omega_{g}i_{qg} \right) \\
\frac{d\Gamma_{q}}{dt} = -\frac{1}{L_{i}} \left( v_{iq} - R_{i}i_{qg} - L_{i}\omega_{g}i_{dg} \right)
\end{cases}$$
(24)

the following formula provides the Lyapunov function:

$$\begin{cases} W_{\beta} = \frac{1}{2} \left( \Gamma_d^2 + \Gamma_q^2 \right) > 0 \\ \frac{dW_{\beta}}{dt} = \Gamma_d \frac{d\Gamma_d}{dt} + \Gamma_q \frac{d\Gamma_q}{dt} \end{cases}$$
 (25)

Furthermore, to ensure the system's stability, the coefficients  $\Upsilon'_d$  and  $\Upsilon'_q$  must be positive.

$$\frac{dW_{\beta}}{dt} = -Y_d'\Gamma_d^2 - Y_q'\Gamma_q^2 < 0 \tag{26}$$

The tracking errors of the grid currents can be attained provided that the d/q voltage references are selected:

$$\begin{cases} v_{id}^* = L_i Y_d' \Gamma_d + \frac{d i_{dg}^*}{d t} + v_g + R_i i_{dg} - L_i \omega_g i_{qg} \\ v_{iq}^* = L_i Y_q' \Gamma_q + R_i i_{qg} + L_i \omega_g i_{dg} \end{cases}$$

$$(27)$$

#### 4. MODEL PREDICTIVE CONTROL

The predictive control approach, specifically model predictive control (MPC), has gained significant importance in power converters and electric drive systems [27], [28]. MPC utilizes a mathematical model for predicting how a process will behave in the future in relation to a certain control variable. The goal is to determine the optimal action by minimizing a predefined cost function, based on set optimization criteria. One variant of MPC, known as predictive deadbeat control, adjusts the control variable rapidly to match the reference input. However, it is sensitive to changes in system parameters and disturbances. In contrast, MPC is favored for its ability to effectively handle complex, nonlinear systems with constraints, as it predicts system behavior using a mathematical model and optimizes control actions accordingly [29].

There are two types of MPC for power converters: continuous control set MPC (CCS-MPC) and FCS-MPC. A modulator is necessary for CCS-MPC to flip between states, ensuring a consistent switching frequency. However, it faces challenges due to the complexity of optimization problems arising from model nonlinearities. The discrete feature of static converters, which have a limited quantity of states that switch, is exploited by FCS-MPC. This reduces the computational demands for prediction and processing. In FCS-MPC, these discrete states are the only states that can be predicted; the ideal state or voltage vector for control is chosen in an optimization stage. The effectiveness of this method depends on an accurate system model and a well-defined cost function. The implementation of FCS-MPC consists of four key steps [30], [31]:

- a. Reference calculation: depending on the particular application, this phase entails determining the reference control value  $x^*(k)$ , which may be torque, flux, power, voltage, and current.
- b. Prediction: Here, the converter switching state combinations S(K), system characteristics, and the discrete time (DT) model are used to predict the future values of the control variables  $x_p(k+1)$ .
- c. Extrapolation: In this stage, present and past sample values  $x^*(k)$ ,  $x^*(k-1)$  are used to predict the future value of the reference control variable  $\hat{x} * (k+1)$ .
- d. Cost function minimization: This function, represented as  $J = \hat{x} * (k+1) x^P(k+1)$ , seeks to minimize the error between the predicted and extrapolated references.

## 4.1. MPC using finite control set for MSC

The discrete PMSG model is used by the MPC algorithm. To simplify the analysis, a forward Euler approximation approach, which takes in consideration the future sample (k + 1) as well as the present sample (k), is adopted in this study. This approach is given as [32]:

$$\left\{\frac{dx(t)}{dt}\right\}_{t=kT_S} \approx \frac{x(kT_S + T_S) - x(T_S)}{T_S} \; ; \; \; x \in \left\{i_{sd}, i_{sq}\right\}$$
 (28)

The (28) may be made simpler as:

$$x(k+1) \approx x(k) + T_s \left\{ \frac{dx(t)}{dt} \right\}_{t=k}$$
 (29)

Following the necessary discretization process, the DT model of the PMSG can be given as [23]:

$$\begin{bmatrix} i_{ds}(k+1) \\ i_{qs}(k+1) \end{bmatrix} = \phi(k) \begin{bmatrix} i_{ds}(k) \\ i_{qs}(k) \end{bmatrix} + \Delta_b \begin{bmatrix} v_{ds}(k) \\ v_{qs}(k) \end{bmatrix} + \Delta_{\overline{w}}(k)$$
(30)

with:

$$\begin{cases}
\phi(k) \approx [I + A(k)T_s] \approx \begin{bmatrix}
1 - \frac{R_s T_s}{L_{ds}} & \frac{\varpi_e(k)L_{qs}T_s}{L_{ds}} \\
-\frac{\varpi_e(k)L_{ds}T_s}{L_{ds}} & 1 - \frac{R_s T_s}{L_{qs}}
\end{bmatrix} \\
\Delta_b \approx BT_s \approx \begin{bmatrix}
\frac{T_s}{L_{ds}} & 0 \\
0 & \frac{T_s}{L_{qs}}
\end{bmatrix} \\
\Delta_\varpi \approx \varpi(k)T_s \approx \begin{bmatrix}
0 \\
-\frac{\varpi_e(k)\psi_r T_s}{L_{qs}}
\end{bmatrix}$$
(31)

Taking into account the DT model of the PMSG as described by (30), the future states of the PMSG currents are forecasted by determining their subsequent values. Consequently, the forecasted direct and quadrature (dq) axis currents can be delineated as [33]:

$$\begin{bmatrix} i_{ds}^{\alpha}(k+1) \\ i_{ds}^{\alpha}(k+1) \end{bmatrix} = \phi(k) \begin{bmatrix} i_{ds}(k) \\ i_{ds}(k) \end{bmatrix} + \Delta_b \begin{bmatrix} v_{ds}^{\alpha}(k) \\ v_{ds}^{\alpha}(k) \end{bmatrix} + \Delta_{\varpi}(k)$$
(32)

where the variable's predicted value is indicated by the superscript  $\alpha$ .

The MSC voltage predictions,  $v_{ds}$  and  $v_{ds}$ , are derived based on switching states and the DC-link voltage ( $V_{dc}$ ) through the model described as:

$$\begin{bmatrix} v_{ds}^{\alpha}(k) \\ v_{qs}^{\alpha}(k) \end{bmatrix} = V_{dc}(k) \begin{bmatrix} S_{ds}^{\alpha}(k) \\ S_{qs}^{\alpha}(k) \end{bmatrix}$$
(33)

The voltage across the capacitor is denoted by  $u_c(k)$ , and  $S_{s,dq}^{\alpha}(k)$  signifies the state of switching along the d/q axis. The formal expression is presented as:

$$\begin{bmatrix} S_{ds}^{\alpha}(k) \\ S_{qs}^{\alpha}(k) \end{bmatrix} = \begin{bmatrix} \cos \theta_e(k) & \sin \theta_e(k) \\ -\sin \theta_e(k) & \cos \theta_e(k) \end{bmatrix}^{\frac{1}{3}} \begin{bmatrix} 1 & -\frac{1}{2} & -\frac{1}{2} \\ 0 & \frac{\sqrt{3}}{2} & -\frac{\sqrt{3}}{2} \end{bmatrix} \begin{bmatrix} S_{sa}^{\alpha}(k) \\ S_{sb}^{\alpha}(k) \\ S_{sc}^{\alpha}(k) \end{bmatrix} \tag{34}$$

By incorporating (32) into (33), we derive the model for the predicted stator currents:

$$\begin{bmatrix} i_{ds}^{\alpha}(k+1) \\ i_{ds}^{\alpha}(k+1) \end{bmatrix} = \phi(k) \begin{bmatrix} i_{ds}(k) \\ i_{ds}(k) \end{bmatrix} + \Delta_b \left( u_c(k) \begin{bmatrix} S_{ds}^{\alpha}(k) \\ S_{ds}^{\alpha}(k) \end{bmatrix} \right) + \Delta_{\varpi}(k)$$
(35)

Conversely, the current references at the (k) sampling instant are projected to the (k + 1) sampling instant through the application of first-order Lagrange extrapolation [34].

$$\begin{cases} \hat{i}_{ds}^*(k+1) = 2i_{ds}^*(k) - i_{ds}^*(k-1) \\ \hat{i}_{gs}^*(k+1) = 2i_{gs}^*(k) - i_{gs}^*(k-1) \end{cases}$$
(36)

In this situation,  $\hat{i}_{sd}^*$  represents the extrapolated reference currents, and  $\hat{i}_{sq}^*$  signifies the generator's reference currents. Under all operational conditions, the direct current  $i_{sd}^*$  is set to zero in order to preserve a unity power factor. Meanwhile,  $i_{sq}^*$  is determined through MPPT control. Ultimately, to reduce the discrepancy between the predicted and extrapolated reference currents, the following cost function is implemented [35]:

$$J_{MSC}(k) = \left[\hat{i}_{ds}^{*}(k+1) - i_{ds}^{\alpha}(k+1)\right]^{2} - \left[\hat{i}_{qs}^{*}(k+1) - i_{qs}^{\alpha}(k+1)\right]^{2}$$
(37)

# 4.2. MPC using finite control set for GSC

Using the same method applied to establish the MSC predictive controller, the GSC cost function can be formulated as [35]:

$$J_{GSC}(k) = \left[\hat{i}_{dg}^*(k+1) - i_{dg}^{\alpha}(k+1)\right]^2 - \left[\hat{i}_{gg}^*(k+1) - i_{gg}^{\alpha}(k+1)\right]^2$$
(38)

Figure 3 depicts the overall framework of the MPC applied to the PMSG wind energy conversion system.

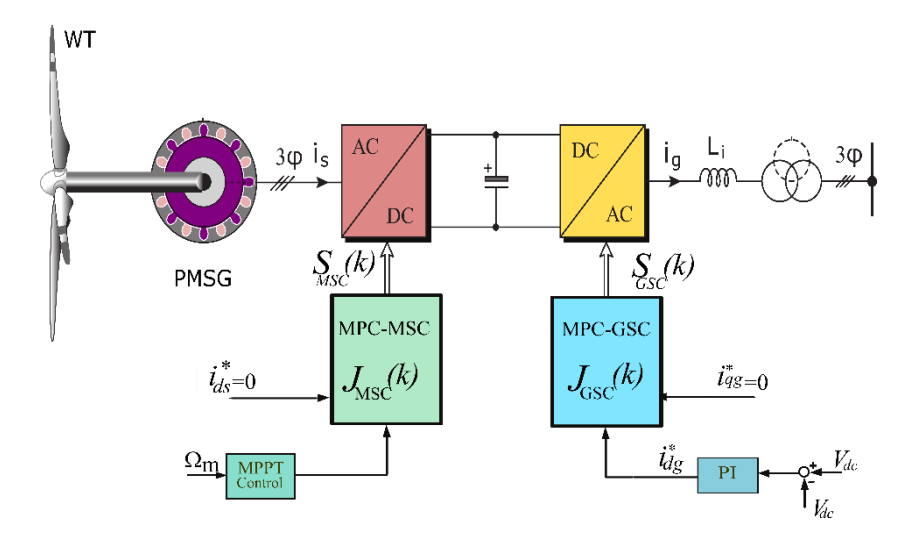


Figure 3. Overview diagram of MPC implementation in the PMSG wind energy conversion system

# 5. RESULTS AND DISCUSSION

This study compares two advanced control strategies, BSC and MPC for controlling both MSC and GSC in a permanent magnet synchronous generator (PMSG)-based WTS connected to the power grid. The wind turbine operates with variable wind speeds between 8.9 m/s and 12.15 m/s as shown in Figure 4, and the system's parameters are outlined in Table 2.

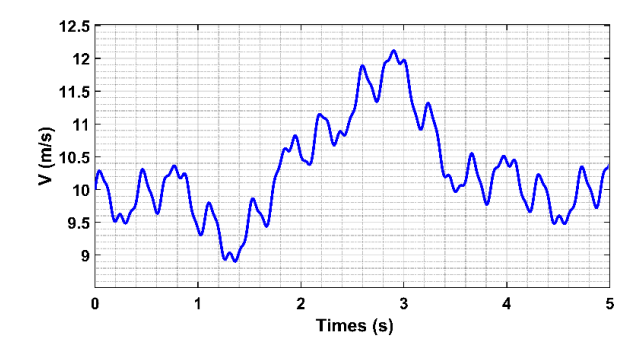


Figure 4. Wind profile

Table 2. Performance comparison: backstepping vs FCS-MPC

Metric	BSC	FCS-MPC
Settling Time (Speed)	0.42 s	0.31 s
Overshoot (Torque)	5.8%	2.3%
Steady-State Error	2.7 rpm	0.9 rpm
THD (Grid Current)	0.47%	0.21%
Std. Dev. (Torque)	1.38 Nm	0.79 Nm
Computation Time/Step	< 0.4 ms	> 1.2 ms

# 5.1. Key findings

The primary aim of this study was to compare the performance of two advanced control strategies used in grid-connected wind energy systems: the FCS-MPC and the standard nonlinear BSC. This comparison was conducted under varying wind conditions and system parameter fluctuations to evaluate the robustness and effectiveness of each approach in realistic operating environments. The FCS-MPC strategy leverages predictive modeling and optimization to anticipate system behavior and select optimal control

actions in real-time. This enables it to achieve superior performance in both dynamic and steady-state conditions. In particular, it demonstrated better tracking of set points and more reliable control during disturbances and parameter variations. In contrast, the BSC approach, while nonlinear and mathematically rigorous, is less computationally demanding but does not incorporate predictive features. As a result, BSC showed limitations in maintaining optimal performance under rapidly changing conditions, highlighting the trade-off between control precision and computational complexity.

# 5.2. Set point tracking scenario

In the scenario of set point tracking, the wind speed was varied according to the profile shown in Figure 4, leading to changes in the generator's mechanical speed. As shown in Figure 5(a), the PMSG speed curves closely follow the wind profile but exhibit smoother dynamics due to the high machine inertia. Both control strategies successfully ensured the WT extracted maximum power, confirming the effectiveness of the MPPT method. However, better tracking was demonstrated by the FCS-MPC approach, guaranteeing more reliable performance in a range of wind situations.

Figure 5(b) shows the PMSG torque, which mirrors the mechanical speed. The torque is smoother with MPC control, reducing mechanical stress and enhancing the turbine's longevity. The reduction in torque ripples indicates the effectiveness of both control strategies, but MPC provided a more consistent and smoother torque profile, leading to better performance in terms of reducing mechanical wear.

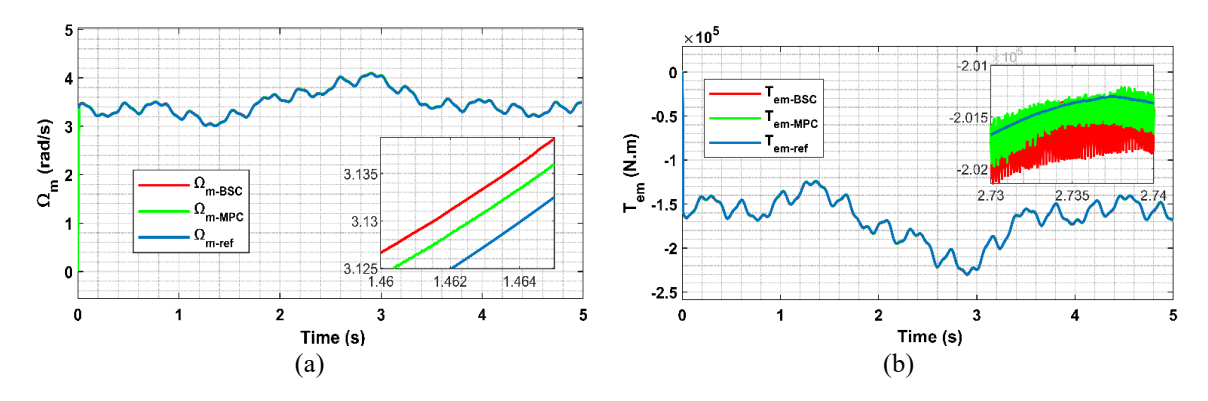


Figure 5. PMSG (a) mechanical speed and (b) electromagnetic torque

# 5.3. Current control performance

Figures 6(a) and 6(b) show the machine-side direct and quadrature currents. While the direct current oscillates around zero (Figure 6(a), the quadrature current Figure 6(b)) is proportional to the electromagnetic torque. The MPC strategy follows the reference current profiles more precisely than BSC, highlighting its superior control accuracy and predictive capabilities. The smooth response of the MPC strategy ensures optimal operation with minimal deviation from the desired values.

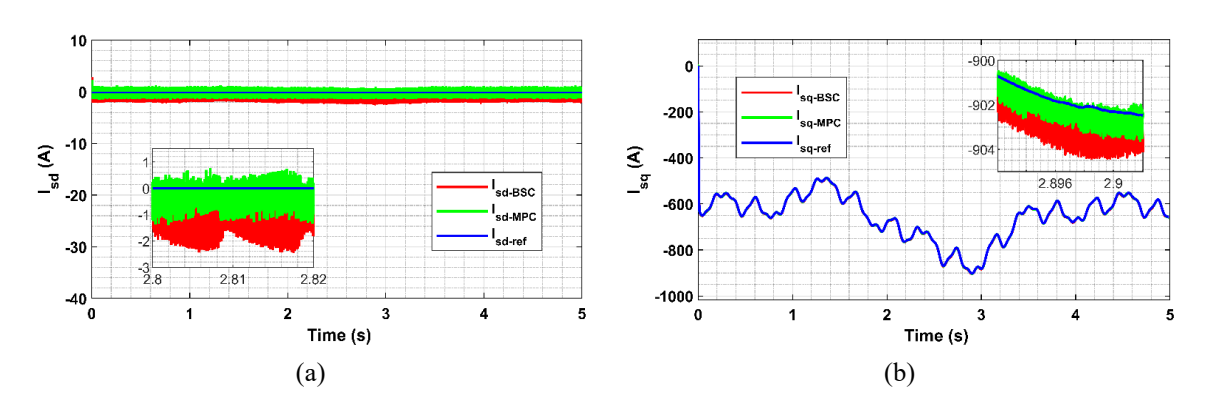


Figure 6. Comparison of stator current tracking performance (a) machine-side direct current and (b) machine-side quadrature current

Figures 7(a) and 7(b) depict the grid-side currents. Both direct  $(i_{gd})$  and quadrature  $(i_{gq})$  components of the grid current track their references effectively with the FCS-MPC strategy. The minimal fluctuation in these currents indicates high power quality and efficient grid integration. To guarantee zero reactive power, the  $i_{gq}$  current is kept at zero, while  $i_{gd}$  represents the active power injected into the grid. MPC control ensures that power injection remains within acceptable limits for both voltage and frequency, confirming its suitability for grid-connected applications.

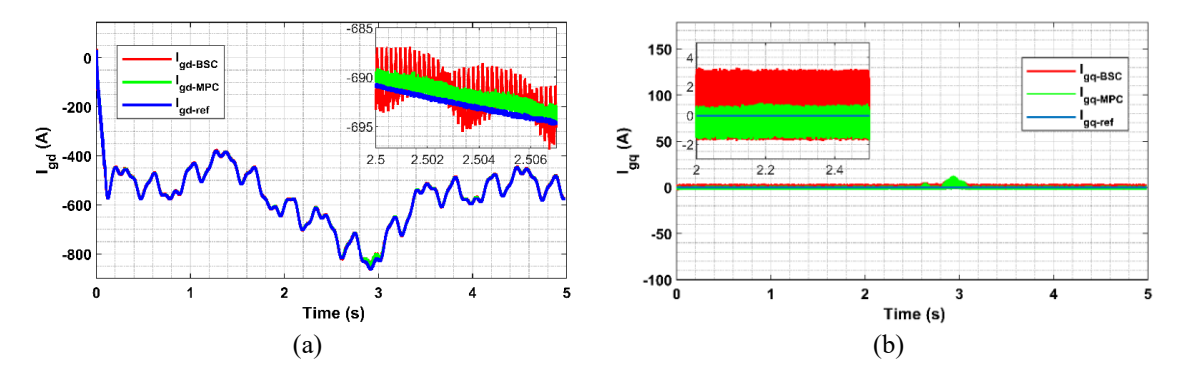


Figure 7. Comparison of grid current tracking performance (a) grid-side direct current and (b) grid-side quadrature current

# 5.4. Power quality

Figures 8(a) and 8(b) present the spectral analysis of the grid-side current, including the total harmonic distortion (THD). Both control strategies meet the IEEE-519.29 standard, with MPC showing slightly better performance (THD of 0.21%) compared to BSC (0.47%). The reduction in harmonic distortion with MPC further demonstrates its enhanced ability to maintain power quality, which is crucial for stable grid operation.

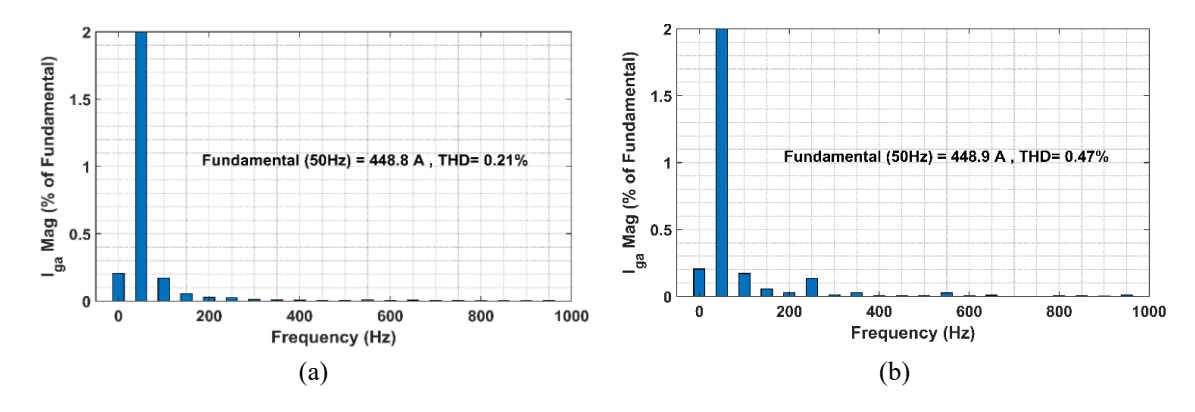


Figure 8. Power quality evaluation based on grid current waveforms THD using (a) MPC and (b) BSC

### 5.5. Discussion and implications

The results from this study underscore the importance of advanced control strategies, particularly MPC, in improving the performance of grid-connected PMSG-based wind turbine systems. MPC's predictive control allows it to adapt dynamically to fluctuations in wind speed and system parameters, providing a more robust solution than the nonlinear BSC approach. While BSC is computationally simpler, it lacks the flexibility and disturbance rejection capabilities of MPC, making it less suitable for systems where high performance and stability under variable conditions are essential. Our findings align with previous research, which suggests that while traditional control strategies like BSC are effective in steady-state conditions, MPC provides significant advantages in dynamic environments, particularly in terms of tracking accuracy and robustness to disturbances. The enhanced power quality and smooth torque profiles achieved with MPC support these conclusions, emphasizing its potential for real-world applications in renewable energy systems.

One of the key strengths of this study is its comprehensive evaluation of both control strategies under varying conditions. However, it is worth noting that the implementation of MPC requires more computational resources compared to BSC, which could pose challenges in systems with limited processing power. Future research could focus on optimizing the computational efficiency of MPC or investigating hybrid control strategies that combine the strengths of both approaches.

# 5.6. Performance metrics and statistical validation

To comprehensively evaluate the performance of the two nonlinear control strategies BSC and FCS-MPC, we analyze key transient and steady-state indicators, including rise time, settling time, overshoot, THD, and statistical deviation under variable wind profiles and parameter deviations. Table 3 summarizes the comparative performance across these criteria, where the FCS-MPC controller demonstrates superior performance in most categories.

Table 3. PMSG-WTS parameters

Parameters	Values	Parameters	Values
Radius	R= 24 m	Flux	$\psi = 6.53 \text{ wb}$
Total inertia	$J=60 \text{ kg.m}^2$	Pair poles	P = 26
Maximum power coefficient	$Cp_{max} = 0.4745115$	DC bus voltage	$V_{dc} = 1500 \text{ V}$
Optimal tip-speed ratio	$\lambda_{\text{optimal}} = 8.101$	DC bus capacitor	$C = 800010^{-6} F$
Nominal power	$P_n = 750 \text{ Kw}$	Filter resistance	$R_{\rm f} = 0.2 \ \Omega$
Stator resistance	$Rs = 6.52.10^{-3} \Omega$	Filter inductance	$L_{\rm f} = 2.10^{-3}  {\rm H}$
Stator inductance	$L_s = L_d = L_q = 3.85.10^{-3} \text{ H}$	Grid nominal voltage	$V_{g} = 400 \text{ V}$

The results indicate that the FCS-MPC approach not only achieves faster convergence and lower overshoot but also ensures superior power quality through reduced THD. The statistical standard deviation of torque further confirms the smoother dynamic behavior of FCS-MPC. However, it is worth noting that these performance gains come at the cost of increased computational complexity. To ensure fairness, all simulations were conducted under identical wind profiles and parameter conditions. While BSC remains computationally efficient and suitable for resource-constrained platforms, FCS-MPC is more effective in highly dynamic environments requiring fine-grained control.

# 6. CONCLUSION AND FUTURE WORK

In this paper, we have studied and compared two nonlinear control strategies, with the aim of developing and adopting the best nonlinear control for a PMSG-based variable-speed WPCS. Using the MATLAB/Simulink environment, a simulation test was conducted at various wind speeds to validate the effectiveness of the suggested solutions. Two case studies are used to assess the effectiveness and performance of the suggested FCS-MPC in comparison to the backstepping controller: tracking test and frequency analysis. The final results of the simulation demonstrate that the FCS-MPC controller offers high performance during transient operations, particularly during MPPT operations. The both case studies confirm that the FCS-MPC can reach the MPPT quickly with minimum overshoot in case of wind speed variation. However, the THD of the stator currents indicates that the deformation of the stator currents under Backstepping is slightly higher than that of the FCS-MPC controller. Based on these findings, we conclude that FCS-MPC is an effective control strategy for PMSG-based wind energy systems. However, the higher computational cost of FCS-MPC remains a consideration.

For future work, real-time experimental validation on platforms such as dSPACE or FPGA is recommended to confirm simulation results. Furthermore, hybrid strategies that combine MPC with adaptive or AI-based algorithms, such as reinforcement learning, offer promising avenues for enhanced control and adaptability in multi-turbine wind farms and smart grid environments.

# REFERENCES

- [1] Q. Hassan et al., "The renewable energy role in the global energy transformations," *Renewable Energy Focus*, vol. 48, p. 100545, Mar. 2024, doi: 10.1016/j.ref.2024.100545.
- [2] V. Ongoma et al., "Morocco's climate change impacts, adaptation and mitigation—a stocktake," *Regional Environmental Change*, vol. 24, no. 1, p. 14, Mar. 2024, doi: 10.1007/s10113-023-02176-2.
- [3] A. El Kassoumi, M. Lamhamdi, A. Mouhsen, M. Fdaili, A. Mouhsen, and I. Aboudrar, "Nonlinear backstepping control of a PMSG-based wind energy conversion system connected to the grid," in 2024 International Conference on Intelligent Systems and Computer Vision (ISCV), IEEE, May 2024, pp. 1–6, doi: 10.1109/ISCV60512.2024.10620091.
- [4] J. Slimani, A. Kadrani, I. El Harraki, and E. Ezzahid, "Towards a sustainable energy future: modeling Morocco's transition to

- renewable power with enhanced OSeMOSYS model," *Energy Conversion and Management*, vol. 317, p. 118857, Oct. 2024, doi: 10.1016/j.enconman.2024.118857.
- [5] A. El Kassoumi, M. Lamhamdi, A. Mouhsen, and A. Mouhsen, "Maximum power generation and pitch angle control of a PMSG-based WECS connected to the grid," in *International Conference on Digital Technologies and Applications*, 2022, pp. 696–705, doi: 10.1007/978-3-031-02447-4 72.
- [6] Z. Wang, J. Chen, M. Cheng, and K. T. Chau, "Field-oriented control and direct torque control for paralleled VSIs fed PMSM drives with variable switching frequencies," *IEEE Transactions on Power Electronics*, vol. 31, no. 3, pp. 2417–2428, Mar. 2016, doi: 10.1109/TPEL.2015.2437893.
- [7] M. Latifi, I. Ouachtouk, I. Aboudrar, and M. Zegrari, "A comparative study of the ADRC and PI controller of a wind turbine driven by a PMSG," in *International Conference on Electrical Systems & Automation*, 2023, pp. 129–137.
- [8] B. Balasubramanyam, "A fuzzy integrated non-linear backstepping control of a grid connected PMSG wind farm," *Journal Electrical Systems*, vol. 20, no. 3, pp. 1983–1991, 2024.
- [9] B. Majout, et al., "Improvement of PMSG-based wind energy conversion system using developed sliding mode control," *Energies*, vol. 15, no. 5, p. 1625, Feb. 2022, doi: 10.3390/en15051625.
- [10] F. Z. Latrech, A. B. Rhouma, and A. Khedher, "FPGA implementation of a robust DTC-SVM based sliding mode flux observer for a double star induction motor: hardware in the loop validation," *Microelectronics Reliability*, vol. 150, p. 115118, Nov. 2023, doi: 10.1016/j.microrel.2023.115118.
- [11] M. Makhad, M. Zazi, and A. Loulijat, "Nonlinear control of WECS based on PMSG for optimal power extraction," *International Journal of Electrical and Computer Engineering (IJECE)*, vol. 10, no. 3, pp. 2815–2823, Jun. 2020, doi: 10.11591/ijece.v10i3.pp2815-2823.
- [12] Y. Errami, A. Obbadi, S. Sahnoun, and M. Aoutoul, "Nonlinear enhanced control for wind energy generation system-based permanent magnet synchronous generator," *Sustainability*, vol. 16, no. 17, p. 7374, Aug. 2024, doi: 10.3390/su16177374.
- [13] M. Fannakh, M. Larbi Elhafyani, S. Zouggar, and H. Zahboune, "Overall fuzzy logic control strategy of direct driven PMSG wind turbine connected to grid," *International Journal of Electrical and Computer Engineering (IJECE)*, vol. 11, no. 6, pp. 5515–5529, Dec. 2021, doi: 10.11591/ijece.v11i6.pp5515-5529.
- [14] M. N. Amin, M. A. Soliman, H. M. Hasanien, and A. Y. Abdelaziz, "Hybrid PSO-GSA algorithm-based optimal control strategy for performance enhancement of a grid-connected wind generator," *International Journal of Applied Power Engineering (IJAPE)*, vol. 10, no. 2, pp. 151–158, Jun. 2021, doi: 10.11591/ijape.v10.i2.pp151-158.
- [15] J. Hu, Y. Shan, J. M. Guerrero, A. Ioinovici, K. W. Chan, and J. Rodriguez, "Model predictive control of microgrids an overview," *Renewable and Sustainable Energy Reviews*, vol. 136, p. 110422, Feb. 2021, doi: 10.1016/j.rser.2020.110422.
- [16] I. Aboudrar, S. El Hani, H. Mediouni, and A. Aghmadi, "Modeling and robust control of a grid connected direct driven PMSG wind turbine by ADRC," Advances in Electrical and Electronic Engineering, vol. 16, no. 4, Dec. 2018, doi: 10.15598/aeee.v16i4.2952.
- [17] A. Bakbak, H. T. Canseven, M. Ayaz, M. Altintas, and E. Mese, "Maximizing energy extraction from direct grid coupled PMSG for wind energy conversion systems," *IEEE Transactions on Industry Applications*, vol. 58, no. 3, pp. 3888–3900, May 2022, doi: 10.1109/TIA.2022.3160141.
- [18] I. AL-Wesabi et al., "Fast DC-link voltage control based on power flow management using linear ADRC combined with hybrid salp particle swarm algorithm for PV/wind energy conversion system," *International Journal of Hydrogen Energy*, vol. 61, pp. 688–709, Apr. 2024, doi: 10.1016/j.ijhydene.2024.02.325.
- [19] Z. Larabi, K. Ghedamsi, and D. Aouzellag, "Direct drive permanent magnet synchronous generator: design, modeling, and control for wind energy applications," *Periodica Polytechnica Electrical Engineering and Computer Science*, vol. 68, no. 2, pp. 168–177, Apr. 2024, doi: 10.3311/PPee.23602.
- [20] S. Liu, H. Wu, T. Bosma, and X. Wang, "Impact of DC-link voltage control on torsional vibrations in grid-forming PMSG wind turbines," *IEEE Transactions on Energy Conversion*, vol. 39, no. 4, pp. 2631–2642, Dec. 2024, doi: 10.1109/TEC.2024.3394753.
- [21] Y. Akarne, A. Essadki, T. Nasser, and H. Laghridat, "Modeling and control of wind turbine system based on PMSG in grid-connected AC microgrid," in *International Conference on Integrated Design and Production*, 2023, pp. 595–604, doi: 10.1007/978-3-031-23615-0 60.
- [22] M. Fdaili, A. Essadki, I. Kharchouf, and T. Nasser, "Noncontrolled fault current limiter with reactive power support for transient stability improvement of DFIG-based variable speed wind generator during grid faults," *International Transactions on Electrical Energy Systems*, vol. 31, no. 8, Aug. 2021, doi: 10.1002/2050-7038.12955.
- [23] W. S. E. Abdellatif, A. M. Hamada, and S. A. M. Abdelwahab, "Wind speed estimation MPPT technique of DFIG-based wind turbines theoretical and experimental investigation," *Electrical Engineering*, vol. 103, no. 6, pp. 2769–2781, Dec. 2021, doi: 10.1007/s00202-021-01268-8.
- [24] Y. El Mourabit, A. Derouich, A. El Ghzizal, N. El Ouanjli, and O. Zamzoum, "Nonlinear backstepping control for PMSG wind turbine used on the real wind profile of the Dakhla-Morocco city," *International Transactions on Electrical Energy Systems*, vol. 30, no. 4, Apr. 2020, doi: 10.1002/2050-7038.12297.
- [25] Y. El Mourabit et al., "Enhanced performance in PMSG-based wind turbine systems: experimental validation of adaptive backstepping control design," *Energies*, vol. 16, no. 22, p. 7481, Nov. 2023, doi: 10.3390/en16227481.
- [26] A. Fathelkhair, H. Abouobaida, Y. Mchaouar, Y. Abouelmahjoub, K. Oualifi, and H. Akli, "Sensorless nonlinear control based on integral backstepping technique for PMSG- based wind energy conversion system," *IFAC-PapersOnLine*, vol. 58, no. 13, pp. 448–453, 2024, doi: 10.1016/j.ifacol.2024.07.523.
- [27] R. Mishra and T. K. Saha, "Predictive power control of PMSG based WECS: development and implementation for smooth grid synchronisation, balanced and unbalanced grid," *Mathematics and Computers in Simulation*, vol. 215, pp. 323–337, Jan. 2024, doi: 10.1016/j.matcom.2023.08.011.
- [28] G. Mirzaeva and Y. Mo, "Model predictive control for industrial drive applications," *IEEE Transactions on Industry Applications*, vol. 59, no. 6, pp. 7897–7907, Nov. 2023, doi: 10.1109/TIA.2023.3299887.
- [29] M. Schwenzer, M. Ay, T. Bergs, and D. Abel, "Review on model predictive control: an engineering perspective," The International Journal of Advanced Manufacturing Technology, vol. 117, no. 5–6, pp. 1327–1349, Nov. 2021, doi: 10.1007/s00170-021-07682-3.
- [30] C.-H. Lin, S. A. Farooqui, H.-D. Liu, J.-J. Huang, and M. Fahad, "Finite control set model predictive control (FCS-MPC) for enhancing the performance of a single-phase inverter in a renewable energy system (RES)," *Mathematics*, vol. 11, no. 21, p. 4553, Nov. 2023, doi: 10.3390/math11214553.
- [31] T. Li, X. Sun, G. Lei, Y. Guo, Z. Yang, and J. Zhu, "Finite-control-set model predictive control of permanent magnet synchronous motor drive systems—an overview," *IEEE/CAA Journal of Automatica Sinica*, vol. 9, no. 12, pp. 2087–2105, Dec. 2022, doi: 10.1109/JAS.2022.105851.

[32] N. A. Nouraldin, M. Chebaani, L. Számel, S. A. M. Abdelwahab, and W. S. E. Abdellatif, "Experimental investigation of predictive control for PMSM-based wind turbine generation system," *Computers and Electrical Engineering*, vol. 119, p. 109554, Oct. 2024, doi: 10.1016/j.compeleceng.2024.109554.

- [33] M. E. Zarei, D. Ramirez, M. Prodanovic, and G. M. Arana, "Model predictive control for PMSG-based wind turbines with overmodulation and adjustable dynamic response time," *IEEE Transactions on Industrial Electronics*, vol. 69, no. 2, pp. 1573– 1585, Feb. 2022, doi: 10.1109/TIE.2021.3057021.
- [34] M. K. Khan Prince, M. T. Arif, A. Gargoom, M. W. Altaf, and M. E. Haque, "Direct model predictive control of grid connected PMSG based wind energy system with LCL filter," in 2022 IEEE Industry Applications Society Annual Meeting (IAS), IEEE, Oct. 2022, pp. 1–8, doi: 10.1109/IAS54023.2022.9940101.
- [35] Z. Huang, Q. Wei, H. Tao, T. Wu, Y. Xia, and M. Rivera, "A cost function-free modulated model predictive control technique for PMSM by the geometric derivations," *IEEE Journal of Emerging and Selected Topics in Power Electronics*, vol. 12, no. 5, pp. 4865–4875, Oct. 2024, doi: 10.1109/JESTPE.2024.3439726.

#### **BIOGRAPHIES OF AUTHORS**





Mohamed Lamhamdi holds a PhD (2008) in materials and technology of electronics components from Paul Sabatier University Toulouse France. After four years research engineer grand gap rectifier project at STMicroelectronics & GREMAN-University of Tours. In November 2011 he has been an assistant professor at National School of Applied Science Khouribga Morocco, where he became the technical manager of the Electronics Signals and Systems (ESS) Group. In January 2018, he joined the Faculty of Science and Technology in Settat, Morocco, where he became member of the RMI Laboratory (Rayonnement-Matière & Instrumentation). Current research topics include, MEMS sensors for RF applications, materials sciences, intelligent systems and energy. He can be contacted at email: mohamed.lamhamdi@gmail.com.



Ahmed Mouhsen D S S C received his Ph.D degree in electronics from the University of Bordeaux, France, in 1992, and he is currently a professor at Electrical Engineering Department, Faculty of Sciences and Technologies, Hassan I University, Settat, Morocco. His research interests focuses on embedded systems, wireless communications and information technology. Prof. Mouhsen has published more than 50 papers in peer-reviewed journals and referred conference proceedings. He can be contacted at email: ahmed.mouhsen@uhp.ac.ma.



Mohammed Fdaili received his master's degree in electrical engineering in 2016 from the high normal school of technical education, Mohammed V University, Morocco. He earned his Ph.D. in electrical engineering in 2022 from the National High School for Computer Science and Systems (ENSIAS), Mohammed V University, Morocco. His research interests focus on renewable energies, particularly in the field of wind turbines. His current activities include developing advanced control strategies for wind energy conversion systems. He can be contacted at email: mohammed.fdaili@gmail.com.



Imad Aboudrar born in Agadir, Morocco, is an Associate Professor of Electrical Engineering at Ibn Zohr University's Higher School of Technology in Dakhla and the chair of ICESST 2024. He holds an M.Sc. from Mohammed V University and completed his Ph.D. in 2021. Dr. Aboudrar has authored more than 26 publications and actively supervises Ph.D. students. He contributes as a reviewer for IEEE, Springer, and Elsevier and has supported and organized key conferences, including, ICESST, ICEIT and CISTEM conferences. He also worked as an R&D Electrified Powertrain Engineer at FEV North Africa, for Stellantis E-Mobility Projects in North America. This industry experience has enriched his academic perspective, particularly in areas of practical application. His research, focused on E-mobility, green hydrogen, and smart microgrids, reflects a commitment to sustainable energy innovation. He can be contacted at email: i.aboudrar@uiz.ac.ma



Azeddine Mouhsen was born on 10 July 1967. He has been a professor of physics at Hassan First University, Morocco, since 1996. He holds a Ph.D. from Bordeaux I University (France) in 1995 and a thesis from Moulay Ismail University, Morocco, in 2001. He specializes in instrumentation and measurements, sensors, applied optics, energy transfer, and radiation matter interactions. He has taught courses in physical sensors, chemical sensors, instrumentation, systems technology, digital electronics, and industrial data processing. He has published over 30 papers, and he is the co-inventor of one patent. Actually, he is the Director of the Laboratory of Radiation-Matter and Instrumentation. He can be contacted at email: azeddine.mouhsen@uhp.ac.ma.